



# A saturation mutagenesis screen uncovers resistant and sensitizing secondary *KRAS*<sup>G12C</sup> mutations to clinical *KRAS*<sup>G12C</sup> inhibitors

Siyu Feng<sup>a,1</sup> , Marinella G. Callow<sup>a</sup> , Jean-Philippe Fortin<sup>b</sup>, Zia Khan<sup>c</sup> , David Bray<sup>d</sup>, Mike Costa<sup>a</sup>, Zhen Shi<sup>e</sup>, Weiru Wang<sup>f</sup> , and Marie Evangelista<sup>a,1</sup>

Edited by David Baker, University of Washington, Seattle, WA; received November 24, 2021; accepted March 14, 2022

Mutant-specific inhibitors of *KRAS*<sup>G12C</sup>, such as AMG510 (sotorasib) and MRTX849 (adagrasib), offer the unprecedented opportunity to inhibit *KRAS*, the most frequently mutated and heretofore undruggable oncoprotein. While clinical data are still limited, on-target mutations in *KRAS*<sup>G12C</sup> at position 12 and other sites are emerging as major drivers of clinical relapse. We identified additional mutations in *KRAS*<sup>G12C</sup> that impact inhibitor sensitivity through a saturation mutagenesis screen in the *KRAS*<sup>G12C</sup> NCI-H358 non-small-cell lung cancer (NSCLC) cell line. We also identified individuals in population genetic databases harboring these resistance mutations in their germline and in tumors, including a subset that co-occur with *KRAS*<sup>G12C</sup>, indicating that these mutations may preexist in patients treated with *KRAS*<sup>G12C</sup> inhibitors. Notably, through structural modeling, we found that one such mutation (R68L) interferes with the critical protein–drug interface, conferring resistance to both inhibitors. Finally, we uncovered a mutant (S17E) that demonstrated a strong sensitizing phenotype to both inhibitors. Functional studies suggest that S17E sensitizes *KRAS*<sup>G12C</sup> cells to *KRAS*<sup>G12C</sup> inhibition by impacting signaling through PI3K/AKT/mTOR but not the MAPK signaling pathway. Our studies highlight the utility of unbiased mutation profiling to understand the functional consequences of all variants of a disease-causing genetic mutant and predict acquired resistant mutations in the targeted therapeutics.

*KRAS*<sup>G12C</sup> | mutagenesis screen | drug resistance | sotorasib | adagrasib

*KRAS* is the most frequently mutated oncogene in human cancer, with mutations detected across many lineages, particularly in the pancreas, colon, and lungs. Among the most commonly activating *KRAS* mutations at codons 12, 13, and 61, G12C occurs in ~13% of lung and 3% of colorectal carcinomas and at lower frequencies in other tumors (1, 2). Despite the high prevalence, the development of therapies that directly target specific *KRAS* mutations has been challenging. However, the landmark discovery of *KRAS*<sup>G12C</sup> inhibitors that covalently modify the mutant Cys12 residue has provided a promising opportunity for drugging *KRAS*<sup>G12C</sup> mutant tumors (3). Currently, multiple *KRAS*<sup>G12C</sup> small-molecule covalent inhibitors have been developed, with sotorasib and adagrasib being the most advanced in the clinical trials. In the most recent data from the sotorasib Phase II trial CodeBreak 100, objective response occurred in 37.1% of the patients, and the median duration of response was 11.1 mo (4). This promising anticancer activity has resulted in accelerated approval from the US Food & Drug Administration for sotorasib in locally advanced or metastatic non-small-cell lung cancer (NSCLC) patients with *KRAS*<sup>G12C</sup> mutations who have received at least one prior systemic therapy.

The emergence of on-target mutations of oncogenes is a common mechanism of acquired resistance in targeted cancer therapies including tyrosine kinase inhibitors and MAPK pathway inhibitors (5–7). Through the analysis of serial cell-free DNA or tumor DNA, recent studies from an adagrasib clinical trial revealed multiple acquired *KRAS* alterations in the resistant patients, including G12D/R/V/W, G13D, Q61H, R68S, H95D/Q/R, and Y96C/D (8, 9). Since amino acids within *KRAS* at positions 12, 68, 95, and 96 are involved in the drug–protein interface (10–12), missense mutations at these positions result in the direct disruption of the binding interaction and resistance to sotorasib and/or adagrasib.

While these observations highlight the ability of a variety of *KRAS* mutations to confer resistance to *KRAS*<sup>G12C</sup> inhibitors, there are likely additional mutations that impact resistance. In this study, we surveyed the impact of all possible amino acid changes within *KRAS*<sup>G12C</sup> on resistance or sensitivity to the *KRAS*<sup>G12C</sup> inhibitors sotorasib and adagrasib. Moreover, additional mutations within *KRAS* may potentially affect drug binding through long-range interactions, modifying intrinsic *KRAS* GTPase

## Significance

*KRAS*<sup>G12C</sup> inhibitors have demonstrated promising efficacy in non-small-cell lung cancer patients harboring the *KRAS*<sup>G12C</sup> mutation. However, the mechanism of resistance remains to be fully understood. To understand the consequences of single amino acid changes within *KRAS*<sup>G12C</sup>, we conducted a saturation mutagenesis screen of the *KRAS*<sup>G12C</sup> protein and assessed the mutational impact on drug sensitivity. Not only did our screen reveal resistant hits that were identified from patients' samples (V8L, C12F, R68S, H95D, H95R, and Y96C), but we also discovered variants that sensitize the inhibition. Furthermore, we examined the human genetics databases and identified germline or somatic *KRAS* mutations that appear among the strong resistance hits. Our study positions future drug discovery targeting *KRAS*<sup>G12C</sup> toward focusing on inhibitors preserving potency against resistance mutations at key residues.

Author contributions: S.F. and M.E. designed research; S.F. and M.G.C. performed research; S.F., J.-P.F., Z.K., D.B., M.C., Z.S., and W.W. analyzed data; and S.F. and M.E. wrote the paper.

Competing interest statement: The authors are current or previous employees of Genentech, Inc. D.B. is an employee of Foundation Medicine, Inc., and is a stockholder of Roche Holding AG.

This article is a PNAS Direct Submission.

Copyright © 2022 the Author(s). Published by PNAS. This open access article is distributed under Creative Commons Attribution-NonCommercial-NoDerivatives License 4.0 (CC BY-NC-ND).

<sup>1</sup>To whom correspondence may be addressed. Email: stefaniefsy@gmail.com or evangelm2@gmail.com.

This article contains supporting information online at <http://www.pnas.org/lookup/suppl/doi:10.1073/pnas.2120512119/-DCSupplemental>.

Published April 26, 2022.

activity, or regulating the interaction between KRAS and downstream effectors. Therefore, a comprehensive understanding of the functional consequences of cooccurring mutations with G12C represents a tremendous unmet need and will bring clinical and scientific benefits for the field of targeted therapy. Here, we designed a saturation mutagenesis screen (Fig. 1A) of the full-length human KRAS<sup>G12C</sup> protein and assessed the mutation impact on drug sensitivity to KRAS<sup>G12C</sup> inhibitors in a human NSCLC model, NCI-H358.

## Results and Discussion

We conducted a saturation mutagenesis screen (Fig. 1A) in NCI-H358 (H358), an NSCLC KRAS<sup>G12C</sup> mutant cell line that carries one copy of KRAS<sup>WT</sup> (WT, wild-type) and one copy of KRAS<sup>G12C</sup> and is highly sensitive to KRAS<sup>G12C</sup> inhibitors (11, 13). We first developed a doxycycline-inducible lentiviral system for KRAS expression and expressed KRAS<sup>G12D</sup>, KRAS<sup>G12C/Q61H</sup>, or KRAS<sup>WT</sup> in H358 to test the ability of these mutations to confer resistance to G12C inhibitors. The most frequently observed KRAS mutation, G12D, leads to a steric hindrance in GTP hydrolysis, impairs the GTPase function, and locks KRAS in its active (GTP-bound) state (14). The Q61H oncogenic mutation has a slightly weaker transforming potential compared to G12D because it demonstrates an extremely slow intrinsic GTP hydrolysis rate (15). We validated the inducible expression of these KRAS variants using Western blot analysis (Fig. 1B). Specifically, in the KRAS<sup>G12D</sup> cell line, the mutant protein KRAS<sup>G12D</sup> was induced and recognized by a RAS<sup>G12D</sup>-specific antibody. In all three inducible cell lines, the levels of KRAS and phospho-ERK1/2 (pERK) proteins were only moderately enhanced compared to the parental line. Through inhibitor treatments, we confirmed the strong resistance phenotype of KRAS<sup>G12D</sup> and the mild resistance phenotype of KRAS<sup>G12C/Q61H</sup> to both sotarasib and adagrasib (Fig. 1C). Before the doxycycline induction of the mutant proteins, the 90% growth inhibition concentration (IC90) of sotarasib and adagrasib in the H358 cell line was 130 nM and 285 nM, respectively. Monitoring the cell growth rate on KRAS<sup>G12C</sup> inhibitors demonstrated that a 13 d culturing conferred a significant growth separation even between the mild resistant (KRAS<sup>G12C/Q61H</sup>) mutant versus the H358-parental line (Fig. 1D). To identify both weak and strong resistant hits, we carried out the screen using KRAS<sup>G12C</sup> inhibitor concentrations at the ~IC90 and exposed cells to chronic treatment for 13 consecutive d.

Having optimized our screening protocol, we then introduced the saturation mutagenesis library containing more than 3,570 missense mutations of KRAS<sup>G12C</sup> into the H358 cells (see *Materials and Methods*). The resistance (or sensitization) mutations were detected through the enrichment (or depletion) of specific variants in the KRAS<sup>G12C</sup> inhibitor treatment groups compared to the DMSO control at the end point of the screen using Z-score heatmap analysis of the log<sub>2</sub> fold change (LFC) of each variant (Fig. 2A and B and *SI Appendix, Table S1*). As a positive control, our data indicated a strict requirement for a Cys residue at the G12 position, ensuring that covalent modification was the key mechanism of inhibition.

The saturation mutagenesis screen identified C12F, R68S, H95D, H95R, and Y96C as strong resistant hits with Z-scores more than 2.5 in the adagrasib-treated groups and is consistent with multiple on-target mutations in KRAS including C12W/F/V, G13D, R68S, H95D/R, and Y96C/D that have been reported in patients who had acquired resistance to the KRAS<sup>G12C</sup> inhibitor

(8, 9). The remarkable consistency between our results and these recent findings supports the clinical relevance of our screen. Surprisingly, we also discovered a subgroup of KRAS<sup>G12C</sup> variants at residues V14, G15, S17, Y32, D33, and M67 that were depleted in the KRAS<sup>G12C</sup> inhibitor-treated groups compared to the DMSO control, suggesting that they may sensitize H358 cells to inhibition.

Using known crystal structures of KRAS<sup>G12C</sup> covalently bound to sotarasib (PDB: 6OIM) and adagrasib (PDB: 6UT0), we next generated contact site maps (*SI Appendix, Fig. S1*) to also highlight mutations that likely alter the inhibitor binding pocket. We indeed observed that across the protein sequence of KRAS, mutations at positions V8, V9, R68, and Y96 were highly enriched in both the sotarasib- and the adagrasib-treated groups.

While there was a similarity in the Z-score heatmaps of the two inhibitors, we also identified several inhibitor-specific mutants. For example, strong enrichment of most substitutions at H95 was identified in the adagrasib-treated groups but not in the sotarasib-treated groups, suggesting that sotarasib binding is compatible with different amino acids at this position whereas adagrasib is less tolerant to changes because it engages a specific hydrogen bond interaction with H95. These observations indicate that the interaction between sotarasib and KRAS<sup>G12C</sup> is less dependent on H95 (*SI Appendix, Fig. S1*) and could be more active against WT HRAS (Q95) or NRAS (L95) compared to adagrasib. A series of Q99 resistance substitutions (Q99F/G/R/S/V/Y) were also specific to the adagrasib-treated group.

We then sought to determine whether any resistant KRAS variants may exist in the human population. While rare, tumors with KRAS<sup>G12C</sup> with these cooccurring preexisting alterations would be expected to show less or no response to the KRAS<sup>G12C</sup> inhibitors. We examined the genome aggregation database (gnomAD) (noncancer samples,  $n = 134,187$ ) and UK Biobank exomes ( $n = 200,643$ ), predicted the germline mutations from the Foundation Medicine (FMI) database ( $n = 327,105$ ), and summarized the total number of KRAS germline variants from three databases as a heatmap (Fig. 2C and *SI Appendix, Table S2*). Although germline nonsynonymous variations in KRAS were indeed rare, several variants found in the human population including V8A, G13E, A59S, and H95N appeared among the strong resistance mutants in either (or both) of the sotarasib- and adagrasib-treated groups. Furthermore, we reasoned that some resistant KRAS mutations may also arise during tumorigenesis and coexist with the G12C allele. From the FMI pan-solid tumor database, we identified a number of G12C cooccurring KRAS mutations (Fig. 2D and *SI Appendix, Table S3*) including V8L, G13E, T58I, R68S, and M72I, which also emerged from our mutagenesis KRAS<sup>G12C</sup> inhibitor screen selection. Together, these data suggest that additional germline or somatic KRAS mutations that confer resistance could be present in KRAS<sup>G12C</sup>-driven tumors and may impact the clinical outcomes of KRAS<sup>G12C</sup> inhibitor treatment.

We next selected a number of resistance (V8A, V8L, V9Y, T58I, A59T, S65W, R68L, R68S, D69P, M72I, D92R, H95N, H95V, Q99F, Q99W, Y96H, and F156L) and sensitizing (S17E) mutations based on Z-scores and frequencies from the human genetic databases (*SI Appendix, Table S4*) for further experimental analysis. We generated individual cell lines, each expressing one of these KRAS mutants through the doxycycline-inducible lentiviral system in the H358 cells. We then performed cell viability assays with dose titration of

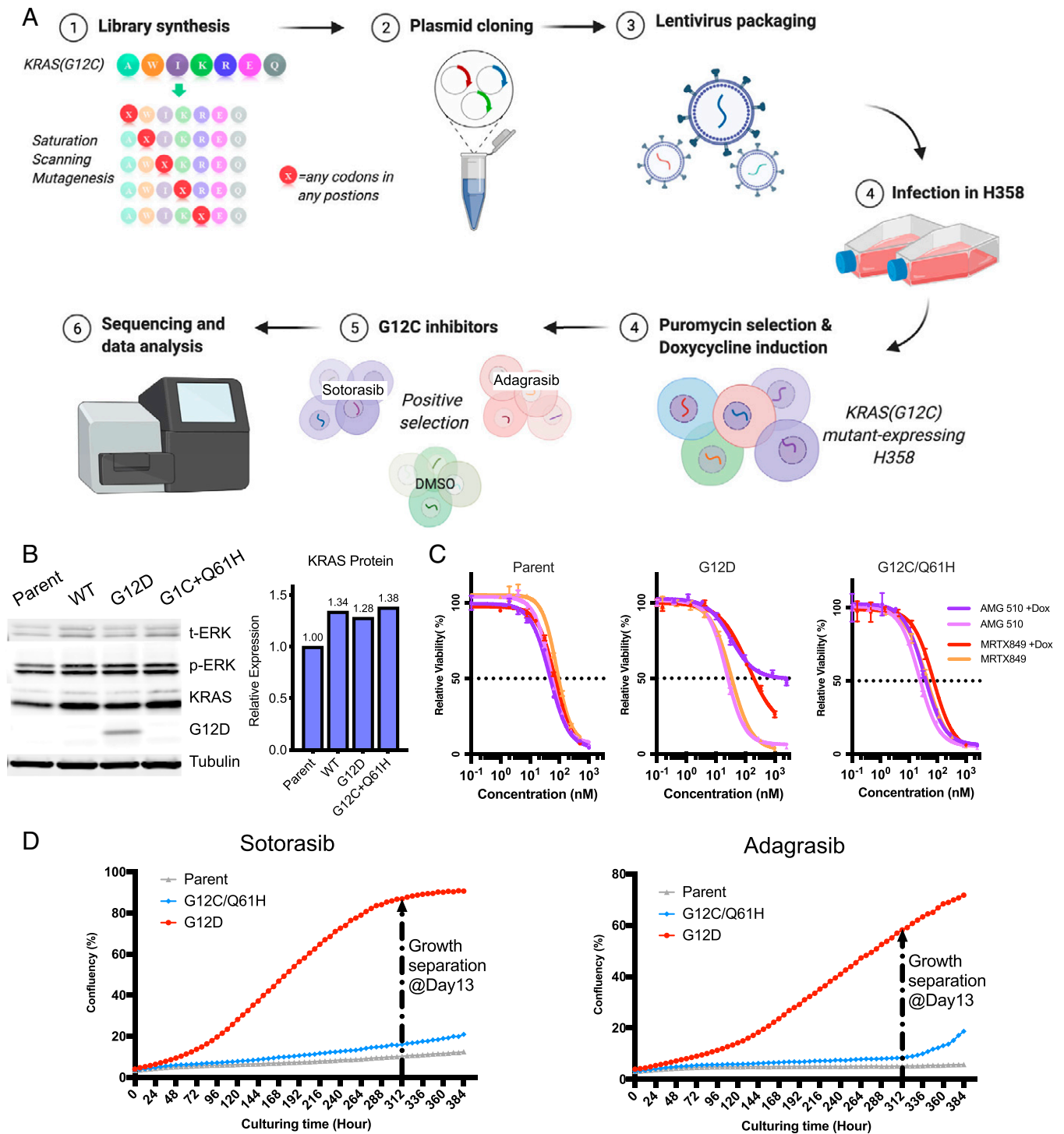


**Fig. 1.** Development of a KRAS saturation mutagenesis screen for KRAS G12C inhibitors in NCI-H358 (NSCLC) cell model. (A) Schematic diagram of the saturation mutagenesis screen. (B) Western blot analysis of engineered H358 cell lines harboring doxycycline-induced KRAS<sup>WT</sup>, KRAS<sup>G12D</sup>, and KRAS<sup>G12C/Q61H</sup> variants. KRAS relative protein level was quantified from the gel image. (C) Cell viability assays for parental H358 and engineered H358 cell lines harboring KRAS<sup>G12D</sup> or KRAS<sup>G12C/Q61H</sup> in culturing conditions with or without doxycycline induction treated with sotorasib and adagrasib for 7 d (shown as mean ± SD,  $n = 3$ ). (D) Cell growth curves of H358 parental and engineered H358 cells expressing KRAS<sup>G12D</sup> or KRAS<sup>G12C/Q61H</sup> under continuous treatment using sotorasib (750 nM) or adagrasib (750 nM) for 16 d. Cell confluency images were acquired every 6 h,  $n = 2$ .

sotorasib or adagrasib in these 18 mutant lines before and after doxycycline induction of the KRAS variants. Most of the mutant cell lines harboring resistance allele mutations demonstrated reduced sensitivity to KRAS<sup>G12C</sup> inhibitors in cell viability studies following induction as indicated by their increased 50% growth inhibition concentration (IC<sub>50</sub>) values, validating their resistant phenotypes to G12C inhibitors (Fig. 2 E–G). In contrast, the S17E mutation demonstrated increased sensitivity

to KRAS<sup>G12C</sup> inhibitors (Fig. 2 E–G). We also observed a strong correlation (nonparametric Spearman correlation  $r = 0.8328$ ,  $P < 0.001$ ) between the screen Z-scores and the IC<sub>50</sub> fold change among the selected mutants.

We next focused on the most significant resistance and sensitization hits, R68L and S17E, respectively, and assessed the functional consequences of these mutations on RAS/MAPK and PI3K/mTOR pathway activity by measuring the pERK and pS6

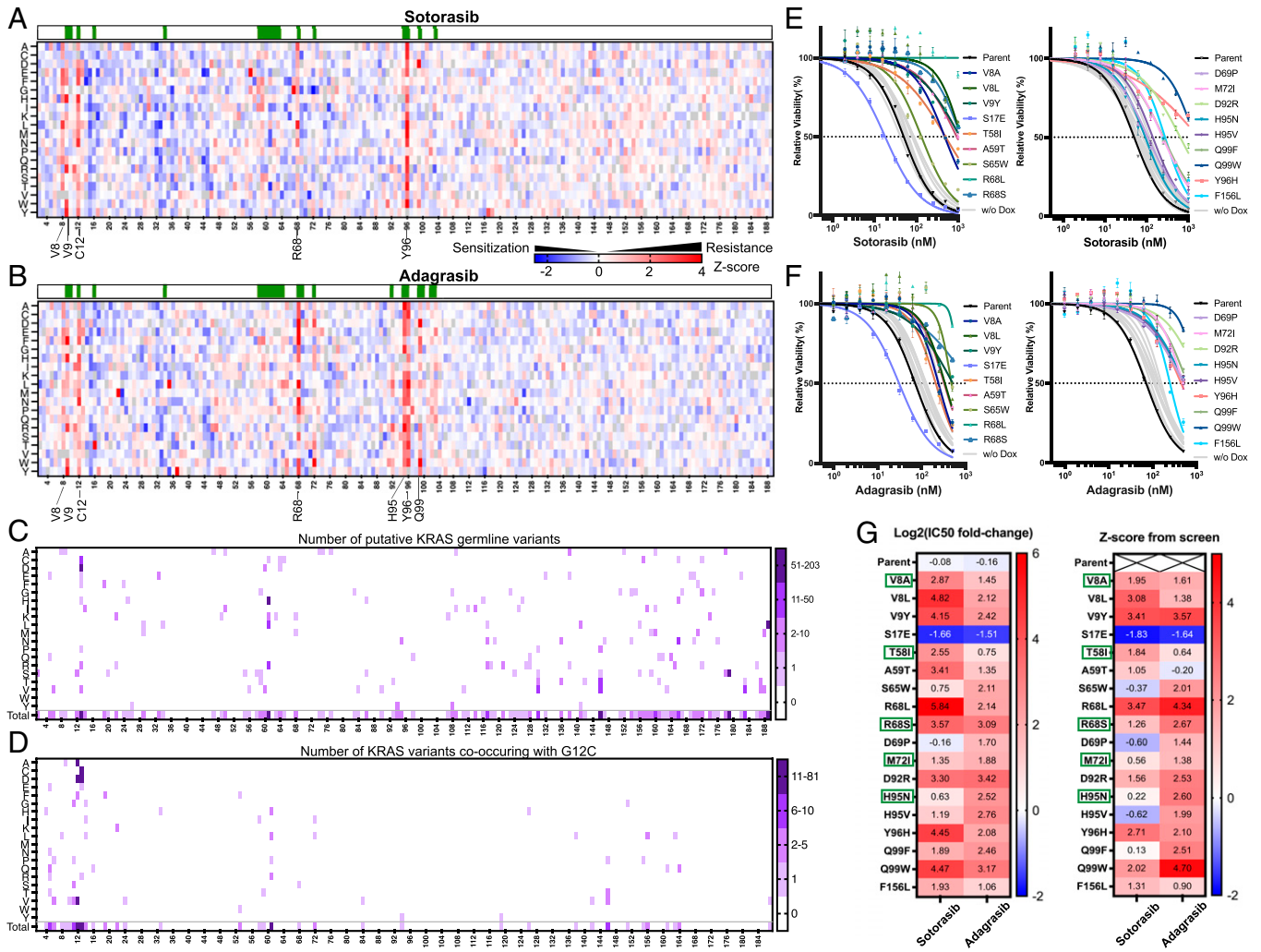


**Fig. 2.** Screen results reveal cooccurring KRAS<sup>G12C</sup> mutations resistant/sensitizing to G12C inhibitors. (A and B) Z-score analysis demonstrating the enrichment (red) and depletion (blue) of all single amino acid substitution mutants of KRAS<sup>G12C</sup> during treatment using sotorasib (A) or adagrasib (B). The green bars above the heatmaps indicate the positions where the KRAS<sup>G12C</sup> protein has direct contact with the inhibitor. (C) Combined number of all KRAS missense mutations that have been reported in noncancer records of the gnomAD and UK Biobank, along with predicted germline mutations from the FMI. The color key indicates the number of individuals combined from these three databases. (D) Number of all secondary mutations that co-occurred with KRAS<sup>G12C</sup> identified in the FMI solid tumor database. The color key indicates the number of individuals. (E and F) Cell viability validation of the resistant/sensitizing phenotypes in H358 by generating 18 cell lines individually expressing KRAS (G12C + secondary mutation). Cells were treated with either sotorasib or adagrasib at indicated concentrations for 7 d after doxycycline induction. (G) Summary of IC50 shift (LFC before and after induction) and screen Z-score for sotorasib or adagrasib treatments in 18 mutant H358 cell lines as well as the parental line. Green boxes indicate mutations also identified in human genetic databases or FMI inquiries.

levels using immunofluorescence imaging. Consistent with the impact on cell viability, the IC<sub>50</sub>, pS6, and pERK levels were both sustained in the resistant KRAS<sup>G12C/R68L</sup> H358 cells (Fig. 3 A and B) under the suboptimal dose (30 nM) of sotorasib or adagrasib, compared to the H358 cells expressing only KRAS<sup>G12C</sup>. Upon increasing the concentrations of KRAS<sup>G12C</sup> inhibitors, we detected partial inhibition of pS6 and pERK in the KRAS<sup>G12C/R68L</sup>-expressing cells; however, complete inhibition was not achieved even at high concentrations ( $\geq 1 \mu\text{M}$ ). Conversely, in the sensitizing mutant KRAS<sup>G12C/S17E</sup>, homogenous and significant pS6 inhibition (Fig. 3 A and C) was observed, even at low concentrations of KRAS<sup>G12C</sup> inhibitors (30 nM), which was not the case in the H358 cells expressing only KRAS<sup>G12C</sup>. Interestingly, the pERK inhibition (Fig. 3B) at various concentrations of KRAS<sup>G12C</sup> inhibitors was similar between the KRAS<sup>G12C/S17E</sup> mutant and the KRAS<sup>G12C</sup> line. This observation suggests that S17E mutation could potentially influence KRAS signaling through PI3K, thereby selectively altering the responsiveness of pS6 signaling (Fig. 3E).

In order to understand the mechanism of resistance for the R68L mutation, we conducted structural modeling of KRAS<sup>G12C</sup> and KRAS<sup>G12C/R68L</sup> mutant proteins bound with sotorasib and adagrasib (Fig. 3D). In the cocrystal structure model with sotorasib, R68 makes a hydrogen bond interaction with the fluorophenol group of sotorasib. The R68 conformation is stabilized by a concurrent salt bridge with D69. The R68L mutation disrupts these interactions by replacing the charged sidechain with a hydrophobic moiety. The situation with adagrasib is distinct because this inhibitor contains a different chemical structure in this region. The crystal structure model shows that R68 adopts an extended conformation and makes two points of contact with the inhibitor. The shorter sidechain in the R68L mutant loses these interactions. Although the details are different, R68L substitution destabilizes the binding between the inhibitor and KRAS<sup>G12C</sup> in both cases. These models exemplify that resistance mechanisms of secondary KRAS mutations could be due to substitutions at key residues directly affecting inhibitor binding (Fig. 3E).

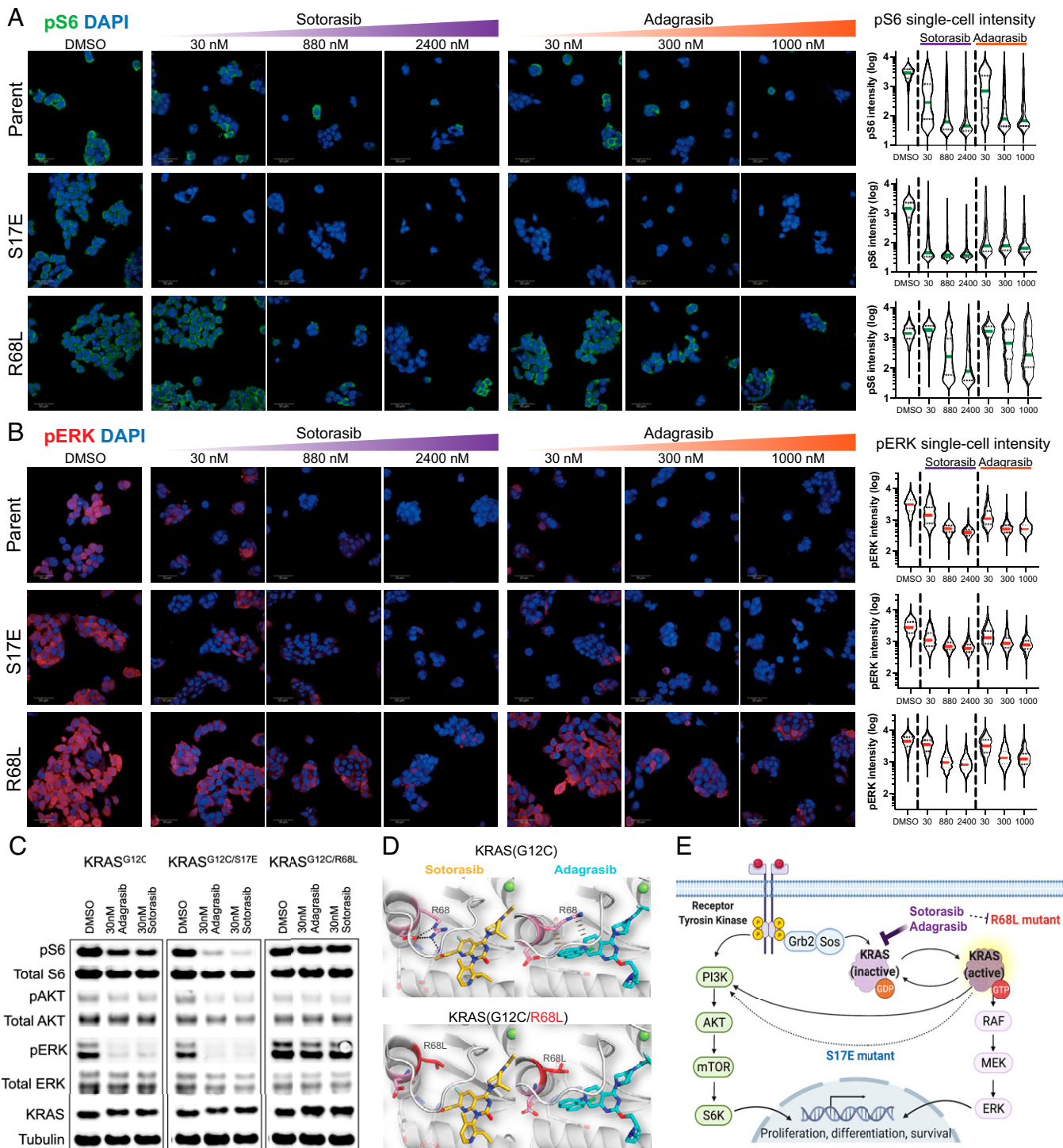


**Fig. 3.** Cellular and structural characterization of selected cooccurring KRAS<sup>G12C</sup> mutants. (A) pS6 immunofluorescence microscopy images and analysis of H358 KRAS<sup>G12C</sup> and mutant KRAS<sup>G12C/S17E</sup> or KRAS<sup>G12C/R68L</sup> cell lines treated with sotorasib and adagrasib at indicated concentrations. Single-cell quantification of pS6 level demonstrates that KRAS<sup>G12C/S17E</sup> line is more responsive in pS6 inhibition, while KRAS<sup>G12C/R68L</sup> line is less sensitive (Scale bar, 50 μM). (B) pERK immunofluorescence microscopy images and analysis of H358 KRAS<sup>G12C</sup> and mutant KRAS<sup>G12C/S17E</sup> or KRAS<sup>G12C/R68L</sup> cell lines treated with sotorasib and adagrasib at indicated concentrations. Single-cell quantification of pERK level demonstrates that KRAS<sup>G12C/S17E</sup> line has a similar baseline level and drug response as the KRAS<sup>G12C</sup> line, while KRAS<sup>G12C/R68L</sup> line has a higher baseline level and less inhibition at suboptimal (30 nM) KRAS<sup>G12C</sup> inhibitor treatment (Scale bar, 50 μM). (C) Western blot result of ERK, AKT, and S6 signaling in KRAS<sup>G12C</sup> mutant cells. H358 KRAS<sup>G12C</sup>, KRAS<sup>G12C/S17E</sup>, or KRAS<sup>G12C/R68L</sup> cell lines were treated with KRAS<sup>G12C</sup> inhibitors at 30 nM for 24 h. (D) Modeled cocrystal structures of sotorasib and adagrasib bound to KRAS<sup>G12C</sup> and KRAS<sup>G12C/R68L</sup>, highlighting the interaction at residue R68 or R68L. (E) Schematic diagram of potential mechanisms of resistant (R68L) or sensitizing (S17E) mutants in the KRAS signaling pathway.

Interestingly, a R68S mutation was identified in the circulating tumor DNA from an NSCLC patient who developed an adagrasib-resistant tumor (9), highlighting that several mutations in this amino acid can impact drug sensitivity.

In summary, we performed an unbiased saturation mutagenesis screen with a full-length human KRAS<sup>G12C</sup> protein and identified numerous mutations that occur in cis with G12C that impacted drug sensitivity to KRAS<sup>G12C</sup> inhibitors in a

human NSCLC model, NCI-H358. Some of these mutations have already been identified in patients who have relapsed on sotorasib and adagrasib. The findings from our saturation mutagenesis screen and of datasets with germline coding variations in KRAS suggest that additional resistance mutations to sotorasib and adagrasib in the clinic will be uncovered over time. Our work also highlights the importance of identifying different chemotypes that differentially bind KRAS<sup>G12C</sup> or pan-KRAS inhibitors to overcome these resistance mechanisms.

## Materials and Methods

**Cell Line and Reagents.** Anti-pERK (Thr202/Tyr204) (#4370, Western blot [WB] 1:2,000; immunofluorescence [IF] 1:400), anti-total ERK (#9107, WB 1:1,000), anti-pS6 (Ser235/236) (#2211, WB 1:1,000), anti-total S6 (#2217, WB 1:1,000), anti-pAKT (Ser473) (#4060, WB 1:1,000), anti-total AKT (#2920, WB 1:1,000), and anti-RAS (G12D Mutant Specific) (#14429, WB 1:1,000) were purchased from Cell Signaling Technology. Anti- $\alpha$ -tubulin (T6199, WB 1:1,000) was purchased from MilliporeSigma. Alexa Fluor 647 Mouse anti-pS6 (pS235/pS236) (560435, IF 1:50) was purchased from BD Biosciences. Alexa Fluor 647 donkey anti-rabbit IgG (711-606-152, IF 1:500) and normal donkey serum (017-000-121) were purchased from Jackson ImmunoResearch Laboratories. Triton X-100 was purchased from Sigma. NucBlue Fixed Cell ReadyProbe Reagent (DAPI) (R37606) and HCS CellMask Blue Stain (H32720) were purchased from Thermo Fisher Scientific. Sotorasib and adagrasib were synthesized in-house as reported in the literature.

The NCI-H358 cell line was acquired through the Genentech internal gCell core facility. Cells were maintained in the RPMI-1640 medium and supplemented with 10% heat-inactivated fetal bovine serum, 1 $\times$  Gibco GlutaMAX (Thermo Fisher, 35050061).

**Library Construction, Lentiviral Production, and Infection.** The human KRAS-4A coding sequence (189 amino acids) was synthesized and cloned into a dox-inducible lentiviral expression vector (Agel/MluI) as the template plasmid. Saturation mutagenesis of KRAS was performed on this template by Twist Bioscience through its DNA Synthesis Silicon platform. The lentiviral expression plasmid library contains all possible single amino acid substitutions of KRAS<sup>G12C</sup>, resulting in more than 3,500 variants. This pooled library was then transfected into GNE 293T cells with packaging plasmid delta8.9 and envelope plasmid VSVG to produce lentiviruses. The virus-containing supernatant was collected 48 h after transfection, clarified by filtering through a 0.45  $\mu$ m syringe, and then concentrated by ultracentrifugation. The lentivirus was then transduced into NCI-H358 cells with 1  $\mu$ g/mL polybrene (TR-1003-G, Sigma-Aldrich) and integrants selected with 1  $\mu$ g/mL puromycin (A1113803, Thermo Fisher).

**Screening Process.** We introduced the saturation mutagenesis library containing more than 3,570 missense mutations of KRAS<sup>G12C</sup> into H358 cells. Three independent lentiviral transductions of the pooled library were conducted in parallel and maintained independently throughout the screen. The multiplicity of infection was kept to  $\sim$ 0.5 to minimize multiple KRAS<sup>G12C</sup> variants in individual cells. Next, 72 h after transduction, successfully integrated H358 cells were selected by supplementing media with puromycin to a final concentration of 1  $\mu$ g/mL. Reference cell pellets were collected the day before puromycin selection. The remaining cells were expanded, and doxycycline (400 ng/mL) was added into the culture medium to induce the expression of KRAS<sup>G12C</sup> variants. In each triplicate, cells were divided into 3 subsets that were treated with sotorasib (750 nM), adagrasib (300 nM), or DMSO, respectively. On day 13, cell pellets were collected and genomic DNA was purified using the Gentra Puregene Kits (Qiagen, 158388). To ensure high-quality sequencing across the entire gene, the KRAS open reading frame (ORF) region was amplified through 2 sets of PCR: one long amplicon (613 bp) covering the whole KRAS gene, and one short amplicon (200 bp) covering the middle region spanning from R68 to A134.

### Bioinformatics and Statistics.

**Amplicon sequencing.** For short amplicons (second round of PCR), single-end (SE) reads of 200 bp length were obtained from an MiSeq instrument using one

lane only. The mean Phred quality score was 38.25, indicating good quality. For the long amplicons (first round of PCR), 250 bp paired-end (PE) reads were obtained from a HiSeq instrument using 2 lanes. Each lane had a mean Phred quality score greater than 35, indicating good quality.

**Alignment of amplicon sequencing reads.** Since the lentiviral ORF constructs were not bar-coded, the full ORF sequences themselves were extracted from the sequencing reads for abundance quantification. To map reads to all possible variants of KRAS ORF sequences, we subdivided each ORF sequence into the 3 following segments: PE sequencing reads of the long amplicons were used to quantify the abundance of mutant ORF with mutations located in either of the 2 outer segments (*SI Appendix, Fig. S2*). Primer sequences were as follows:

```
Outer_fwd: TCGTAAAGTACCGTGCCACCATG
Outer_rev: AGGGACCAGTACATGAGGACTGG
Inner_fwd: GCTAAGTCTGAGCCTGTTTGT
Inner_rev: ATTACTCGGGCCCCACGCGTTTA
```

SE sequencing reads of the short amplicons were used to quantify the abundance of mutant ORF with mutations located in the inner segment. Alignment of both SE and PE reads was performed using an in-house alignment software written in R, allowing only one mismatch between read sequences and the set of bar codes. This resulted in three count matrices, corresponding to each segment.

**Normalization of read counts.** To adjust for the difference in sequencing depth between the SE and PE sequencing data within a sample (within-sample normalization), we equalized the total number of reads that appeared to be identical to the wild-type KRAS<sup>G12C</sup> ORF from the SE sequencing (inner segment) to the total number of reads that mapped to a KRAS G12C mutant ORF in the PE sequencing (outer segments). For between-sample normalization, we performed a standard median equalization to adjust for the difference in sequencing depth between samples and prepared libraries.

**Statistical analysis.** We concatenated the three normalized count matrices into one final count matrix to be used for downstream statistical analyses. We used the Bioconductor Summarized Experiment machinery to store count data and keep track of the feature annotation (16). We used limma-voom to perform a statistical differential analysis of the sequencing counts data (17). The following comparisons were tested: every drug or DMSO versus a reference comparison (e.g., sotorasib vs. reference), and every drug versus a DMSO (e.g., sotorasib vs. DMSO) combination for a total of five comparisons. For each comparison, the limma-voom generated the three following summary statistics for each mutant ORF: an LFC, a *P* value associated with the moderated *t* test statistic, and a false discovery rate (FDR)-corrected *P* value using the Benjamini-Hochberg multiple hypothesis correction method. We then transformed the LFC into a Z-score heatmap where the population mean and SD were taken into consideration to identify statistically significant hits.

**KRAS Genetic Variants in Population Databases.** To examine the mutations in KRAS that may cooccur with G12C, a total of more than 327,000 samples from adult solid tumors in the FMI database (2021 Q1 data freeze) were assessed. A computational algorithm was used to determine the germline versus the somatic origin of KRAS variants, as previously described (18). To explore existing KRAS variants in the human population, the gnomAD (*n* = 134,187) and UK Biobank exomes (*n* = 200,643) and the predicted germline mutations from the FMI database (*n* = 327,105) were examined. Only noncancer samples were used from the gnomAD and UK Biobank databases.

**Stable KRAS Mutant Cell Lines and Cell Viability Assay.** We cloned 18 KRAS<sup>G12C</sup> variant sequences with secondary mutations (V8A, V8L, V9Y, S17E, T58I, A59T, S65W, R68L, R68S, D69P, M72I, D92R, H95N, H95V, Q99F, Q99W, Y96H, and F156L) into the same dox-inducible lentiviral expression vector used in the screen. Stable NCI-H358 mutant cell lines were established through lentivirus infection as described above in the lentiviral production and infection section. For the cell viability assay, cells were dosed with sotorasib and adagrasib in a 10-point dose-response using a twofold dilution series. KRAS mutant cells were seeded into 384-well plates at 1,000 cells per well 24 h before compound addition and incubated with compound for 7 d before assaying viability (CellTiter-Glo, Promega). For the doxycycline-induction groups, 400 ng/mL doxycycline was added during cell seeding. Assays were performed in biological duplicates. Nonlinear regression curves were fitted using Prism 9 software. IC50 (absolute IC50) is the dose at which the estimated viability is 50% relative to

untreated (DMSO) wells. The IC50 shift was calculated as an LFC of IC50 values for each KRAS mutant cell line before or after doxycycline induction.

**Immunofluorescence Staining, Microscopy, and Imaging Analysis.** The KRAS<sup>G12C</sup>, KRAS<sup>G12C/S17E</sup>, and KRAS<sup>G12C/R68L</sup> H358 cells were seeded in poly-D-lysine-coated CellCarrier-96 Ultra microplates (PerkinElmer, 6055500) 24 h before compound addition. In addition, 400 ng/mL doxycycline was added during seeding. Sotarasib and adagrasib were incubated for 20 h with 3 different concentrations (indicated in the Fig. 3 legend). Cells were then fixed with 4% paraformaldehyde for 15 min at room temperature, washed 2× with phosphate-buffered saline (PBS) and then quenched with 50 mM NH<sub>4</sub>Cl (Sigma A4514) for 10 min. Cells were then permeabilized with ice-cold 100% methanol for 10 min at -20 °C and rinsed in PBS for 5 min. Blocking was then performed in the blocking buffer (PBS/5% normal serum/0.3% TritonX-100) for 1 h at room temperature. For pS6 staining, the Alexa Fluor 647 conjugated mouse anti-pS6 (pS235/pS236) antibody was incubated with cells for 1 h at room temperature. For pERK staining, rabbit anti-pERK (Thr202/Tyr204) was incubated with cells for 1 h at room temperature, washed with PBS for 10 min 3×, and then incubated with the Alexa Fluor 647 donkey anti-rabbit secondary antibody for 1 h at room temperature. NucBlue Fixed Cell ReadyProbe Reagent (DAPI) and HCS CellMask Blue Stain were then used together to stain the nuclear and cell body for 30 min. Cells were then washed 3× with PBS and kept in PBS for imaging.

Images were acquired on the Opera Phenix Plus High-Content Screening System (PerkinElmer) using the 40× water immersion (numerical aperture = 1.1) objective and the confocal mode for better resolution. Next, 20 fields of view were acquired for each well to enable the quantitative analysis of fluorescence intensities. Image segmentation, signal intensity quantitation, and single-cell analysis were performed using the Harmony software (PerkinElmer). Cytoplasmic and nuclear areas were identified by using two thresholds on the CellMask Blue Stain (low intensity) and DAPI (high intensity) channels. Single-cell objects were

identified according to successful nuclear segmentation. For both pS6 and pERK immunofluorescence signals, quantifications are average signals of the cytosolic area. Population median value and single-cell data were analyzed using Prism 9 software. Single-cell violin plots were generated using signal intensities for individual cells in Prism 9.

**Structural Modeling.** Computational models of KRAS<sup>G12C</sup> with secondary mutations were built using program Molecular Operating Environment (MOE) based on the crystal structures of KRAS<sup>G12C</sup>/sotarasib (PDB: 6OIM) or KRAS<sup>G12C</sup>/adagrasib (PDB: 6UTO) for the variants related to sotarasib and adagrasib, respectively. The structure was first subject to energy minimization to remove strains. The desired mutation was then modeled with the most favorable rotamer conform considering the crystal structural environment. The mutated structure was then subject to another round of energy minimization. The ligand was maintained bound and allowed to be flexible throughout the modeling process.

**Data Availability.** All study data are included in the article and/or *SI Appendix*.

**ACKNOWLEDGMENTS.** We are thankful to Sushant Malhotra, Zora Modrusan, Yuxin Liang, and Matthew Chang for helpful discussions; Honglin Chen for packaging the lentiviral library; and the staff at the Next-Generation Sequencing group at Genentech for their assistance on amplicon sequencing.

---

Author affiliations: <sup>a</sup>Department of Discovery Oncology, Genentech, Inc., South San Francisco, CA 94080; <sup>b</sup>Department of Bioinformatics, Genentech, Inc., South San Francisco, CA 94080; <sup>c</sup>Department of Human Genetics, Genentech, Inc., South San Francisco, CA 94080; <sup>d</sup>Foundation Medicine, Inc., Cambridge, MA 02141; <sup>e</sup>Department of Oncology Biomarker Development, Genentech, Inc., South San Francisco, CA 94080; and <sup>f</sup>Department of Structural Biology, Genentech, Inc., South San Francisco, CA 94080

1. D. Kim, J. Y. Xue, P. Lito, Targeting KRAS(G12C): From inhibitory mechanism to modulation of antitumor effects in patients. *Cell* **183**, 850–859 (2020).
2. A. H. Nassar, E. Adib, D. J. Kwiatkowski, Distribution of KRAS<sup>G12C</sup> somatic mutations across race, sex, and cancer type. *N. Engl. J. Med.* **384**, 185–187 (2021).
3. J. M. Ostrem, U. Peters, M. L. Sos, J. A. Wells, K. M. Shokat, K-Ras(G12C) inhibitors allosterically control GTP affinity and effector interactions. *Nature* **503**, 548–551 (2013).
4. F. Skoulidis *et al.*, Sotarasib for lung cancers with KRAS p.G12C mutation. *N. Engl. J. Med.* **384**, 2371–2381 (2021).
5. J. A. Engelman, P. A. Jänne, Mechanisms of acquired resistance to epidermal growth factor receptor tyrosine kinase inhibitors in non-small cell lung cancer. *Clin. Cancer Res.* **14**, 2895–2899 (2008).
6. K. Suda *et al.*, Small cell lung cancer transformation and T790M mutation: complimentary roles in acquired resistance to kinase inhibitors in lung cancer. *Sci. Rep.* **5**, 14447 (2015).
7. J. Wang *et al.*, A secondary mutation in BRAF confers resistance to RAF inhibition in a BRAF V600E-mutant brain tumor. *Cancer Discov.* **8**, 1130–1141 (2018).
8. N. Tanaka *et al.*, Clinical acquired resistance to KRAS<sup>G12C</sup> inhibition through a novel KRAS switch-II pocket mutation and polyclonal alterations converging on RAS-MAPK reactivation. *Cancer Discov.* **11**, 1913–1922 (2021).
9. M. M. Awad *et al.*, Acquired resistance to KRAS<sup>G12C</sup> inhibition in cancer. *N. Engl. J. Med.* **384**, 2382–2393 (2021).
10. J. B. Fell *et al.*, Identification of the clinical development candidate MRTX849, a covalent KRAS<sup>G12C</sup> inhibitor for the treatment of cancer. *J. Med. Chem.* **63**, 6679–6693 (2020).
11. J. Canon *et al.*, The clinical KRAS(G12C) inhibitor AMG 510 drives anti-tumour immunity. *Nature* **575**, 217–223 (2019).
12. T. Patsar, KRAS(G12C)-AMG 510 interaction dynamics revealed by all-atom molecular dynamics simulations. *Sci. Rep.* **10**, 11992 (2020).
13. J. Hallin *et al.*, The KRAS<sup>G12C</sup> inhibitor MRTX849 provides insight toward therapeutic susceptibility of KRAS-mutant cancers in mouse models and patients. *Cancer Discov.* **10**, 54–71 (2020).
14. J. C. Hunter *et al.*, Biochemical and structural analysis of common cancer-associated KRAS mutations. *Mol. Cancer Res.* **13**, 1325–1335 (2015).
15. C. Muñoz-Maldonado, Y. Zimmer, M. Medová, A comparative analysis of individual RAS mutations in cancer biology. *Front. Oncol.* **9**, 1088 (2019).
16. W. Huber *et al.*, Orchestrating high-throughput genomic analysis with Bioconductor. *Nat. Methods* **12**, 115–121 (2015).
17. C. W. Law, Y. Chen, W. Shi, G. K. Smyth, voom: Precision weights unlock linear model analysis tools for RNA-seq read counts. *Genome Biol.* **15**, R29 (2014).
18. J. X. Sun *et al.*, A computational approach to distinguish somatic vs. germline origin of genomic alterations from deep sequencing of cancer specimens without a matched normal. *PLOS Comput. Biol.* **14**, e1005965 (2018).